Laser Ablation for Cardiac Tissue Oxygenation

Keywords: modeling, oxygen transfer, laser ablation, myocardium, TMLR

Authors:

Jacqueline Dokko

Chae Young Eun

Conor Kiembock

Qikun Wang

May 19, 2017

BEE 4530: Computer-Aided Engineering

Contents

1 Executive Summary

The leading cause of myocardial infarctions, commonly known as heart attacks, is the reduced blood flow to the heart muscle due to plaque buildup in the coronary artery. Transmyocardial laser revascularization (TMLR) is one of the more recently used procedures to treat blocked arteries when traditional treatments such as vascular stents and bypass grafting surgery are not suited for the patient. TMLR involves a CO_2 laser heating process to ablate heart tissue and create channels through the entire myocardium wall. The new channels throughout the heart then facilitate transport of oxygenated blood from the ventricle to the oxygen-deprived heart tissue shortly after the procedure. After a long time, the heart can revascularize the affected area, healing the channels while simultaneously creating new blood vessels through a process called angiogenesis. Eventually the new blood vessels replenish oxygen in the heart tissue.

Our project goal was to model the tissue ablation and oxygenation process of TMLR and optimize the channel-making procedure. Our quantities of interest were healthy tissue damage and short-term oxygen transfer, which we wanted to minimize and maximize respectively. We used COMSOL® to model the laser heating via the heat transfer module and simplified the procedure domain to a two-dimensional, axisymmetric geometry. Our model simulates the channel formation process through the use of the "Deformed Geometry" feature in COMSOL. Next, we analyzed the oxygen transfer process from the inflowing blood to the surrounding tissue on another two-dimensional, axisymmetric model with a mass transfer equation. Additionally, we coupled fluid flow equations to the mass transfer governing equation to observe the effects of blood flow on the oxygen transfer to the tissue.

In optimizing this procedure, we looked at various combinations of laser power and spot size radii, the two factors that can be varied to deliver different laser heat fluxes to the tissue. Using the two simulation models, we concluded that the optimal laser power is in the range of 538 W to 600 W and optimal spot size radius is 0.55 mm. These laser configurations take into account the negative effects of overheating and the positive effects of oxygen transfer.

The results of this report are significant for the patients who suffer from heart attacks and for the surgeons who are in search of better solutions. The laser heating procedure discussed in this report can serve as an alternative treatment for patients who have already received traditional methods of treating blocked arteries but did not experience significant changes in their symptoms. From the results of our models, we provide promising evidence that revascularization through TMLR successfully oxygenates the myocardial tissue in the short term.

Key words: modeling, oxygen transfer, laser ablation, myocardium, TMLR

2 Introduction

Transmyocardial laser revascularization (TMLR) has been researched extensively. Upon understanding the process at hand, we have set tangible goals and objectives to move forward with the analysis of TMLR, the relevant changes in oxygenation and tissue damage, and the parameters that affect our quantities of interest.

2.1 Background of Problem and Common Treatment

Myocardial infarction, commonly known as a heart attack, is a leading cause of death in the United States and around the world [1]. The myocardium, or the main muscular heart tissue, lacks oxygen supply due to a reduction of blood flow from the arteries in the heart walls, and this may cause a painful condition called angina [2]. In classical surgical treatment of myocardial infarction, natural or artificial blood vessels can be grafted onto the patient's heart during an open heart surgery to remedy blockages of arteries. While this coronary artery bypass surgery has been the most commonly used procedure to address this problem in the past, some patients are not suited for this surgery; as such, different alternatives must be executed for these patients. Due to the nature of this technique, there are many risks that come along with the bypass surgery, including recurring blockages of the arteries, excessive blood loss, and rare cases in which a stroke can be caused from the interference with the arteries that connect to the brain [2]. As such, our research indicates that we can replace these previous techniques with TMLR.

2.2 Review of Mirhoseini's work

In Mirhoseini's research, this alternative method of laser heating to create temporary channels to bring oxygen to the heart tissue was examined [1]. Patients who require the surgery have a lethally low level of oxygen in their blood. The procedure allowed the patient's blood oxygen levels to rise to the minimum viable level and eventually to the normal level. An experiment using a highly variable CO_2 laser to vaporize the channels into the hearts of several groups of dogs was carried out. When the dogs' hearts were examined at various times after the operation, the channels were not burned by the laser, and even remained in the heart for months to continue providing the tissue oxygen. The left anterior descending (LAD) coronary artery was ligated at different points for each group of dogs, with the control group receiving no laser treatment at all, one group receiving laser treatment post ligation, and the other two groups receiving laser treatment before ligating the coronary artery.

The control group had a one hundred percent mortality rate. The group receiving laser treatment before the ligation had zero mortality after the surgery, while the group which had their arteries ligated before any laser treatment had up to sixty percent mortality rate. This experiment demonstrated that the channels formed by the laser could effectively keep the animals alive by supplying oxygenated blood to the heart, even without the LAD

coronary artery [1].

While Mirhoseini's experiment varied the amount of channels per unit area between two groups, it did not examine the effects of changing laser power [1]. We filled in this missing information by varying the laser power and demonstrated possible positive and negative effects of increasing or decreasing the power. Additionally, Mirhoseini showed oxygen was being supplied to the tissue inductively, illustrating that since the dogs lived and the channels were still visible in their hearts after examination, that oxygen must have diffused into the tissue. While this is certainly true, we took a step further and demonstrated quantitatively how well oxygen diffuses from the channel into the tissue [1].

2.3 Current Research

Currently, the transmyocardial revascularization procedure is used to treat scarred myocardial tissue in conjunction with cell therapy to enhance recovery. Clinical trials combining the laser therapy with cell grafting have been showing positive effects. Thus, more research is being conducted to uncover the mechanism of the dual therapy that allows for the increased alleviation of myocardial complications [3]. Analysis of the molecular scale metabolic effects of TMLR will be required to achieve this goal. Therefore, it was appropriate for us to understand and model not only the laser treatment portion of this procedure, but also the oxygen diffusion as a result of the channel formation.

Slight deviations from this model as such as counterpulsation therapy are being tested as alternatives, as well [4]. Unsurprisingly, there have been recent software-based attempts to model the procedure. However, instead of visually analyzing the process, researchers have modeled the quantitative aspects of TMLR such as optimal number of holes, perfusion from a single hole, and threshold power using MATLAB® and C++® [5].

2.4 Problem Statement

Currently, there is a lack of a comprehensive model for the heat and mass transfer processes of TMLR. The development of a computational model could greatly alleviate the experimentation required to refine the procedure protocol. Thus, our group developed two dimensional, axisymmetric models to simulate the ablation and oxygenation of the myocardial tissue.

2.5 Design Objectives

Our goal was to create 2-D, axisymmetric models of the tissue ablation and oxygenation in COMSOL® to simulate the laser heating and oxygen transfer procedures. Using these model, we optimized the laser power and spot size applied to the tissue so that the heart

muscle where the channel is to be created is successfully ablated while minimizing the destruction of healthy tissues in the proximity. We also analyzed the new oxygen diffusion profile in the tissue after the channel has been created and blood has flown through it to ensure that the procedure increased oxygen concentration in the heart. Our objectives were to:

1. Develop a 2-D axisymmetric model of the left ventricular wall with cardiac tissue and CO_2 laser on COMSOL.
2. Implement the time-dependent heat transfer model of the laser ablation through the tissue, including the boundary conditions, initial conditions and moving boundary of the laser surface, and simulate the channel-making process.
3. Modulate the CO_2 laser power and laser spot size to minimize damage to healthy tissue around the affected area. This was done with the use of an objective function that assigns high function values when healthy tissue outside of the channel is either damaged or ablated. Damage was defined by temperatures above 60°C and ablation was defined by temperatures above 100°C [6,7].
4. Model the change in oxygen concentration throughout the cardiac tissue after surgical recovery and evaluate the short-term efficacy of the procedure.

3 Problem Formulation

The development of an accurate model requires understanding of the process itself and the calculations which involves governing equations, boundary and initial conditions, and properties of the materials involved.

3.1 Process Demonstration

The laser must ablate through cardiac tissue and the tissues that compose the blood vessel in order for the vessels to revascularize and recover in the form of smaller, unblocked vessels [8] as shown in the third panel of Figure 1.

3.2 Schematics

The ablation was modeled using a 2-D, axisymmetrical geometry with a uniform slab of myocardial tissue as shown in Figure 2. Because blood and the myocardium tissue have similar property values, we excluded the blood vessel in our model.

The mass transfer portion of the procedure was also modeled as a 2-D axisymmetric model due to its symmetry. Similarly to the heat transfer model, the axis for this model is the center of the channel as seen in Figure 3.

Since both the heat transfer and mass transfer models were developed with 2-D axisymmetry, the parallel between the channel ablation and the subsequent oxygen transfer via blood flow can be drawn easily.

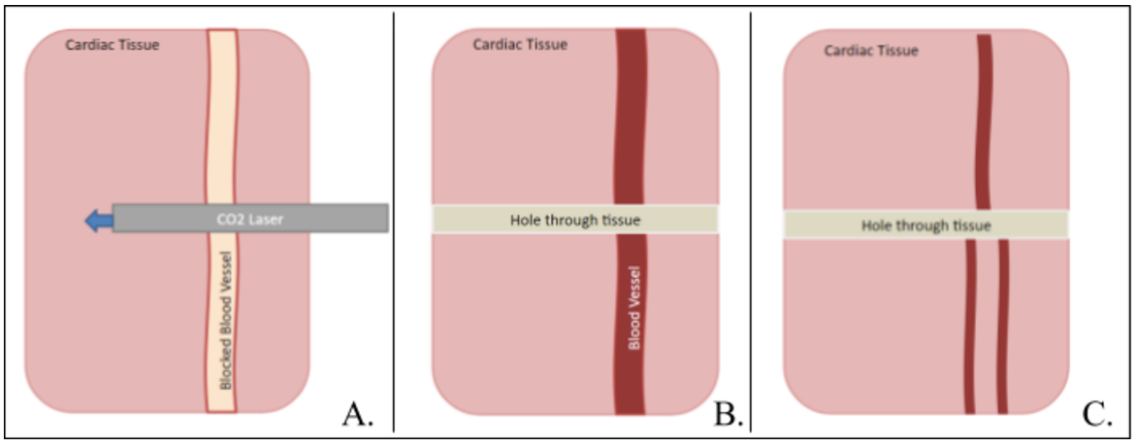

Figure 1: Step-by-step process of laser creating the channel through the heart tissue and blood vessel. A constant laser flux is applied in Fig.1.A., vaporizing cells in its path. In Fig.1.B. , we see the completed channel from the outside of the heart to the ventricle, and in Fig.1.C., we observe new blood vessel formation after a long period of time, where genesis of new vessels has occurred, successfully revascularizing the tissue to provide long-term oxygen flow to the myocardium.

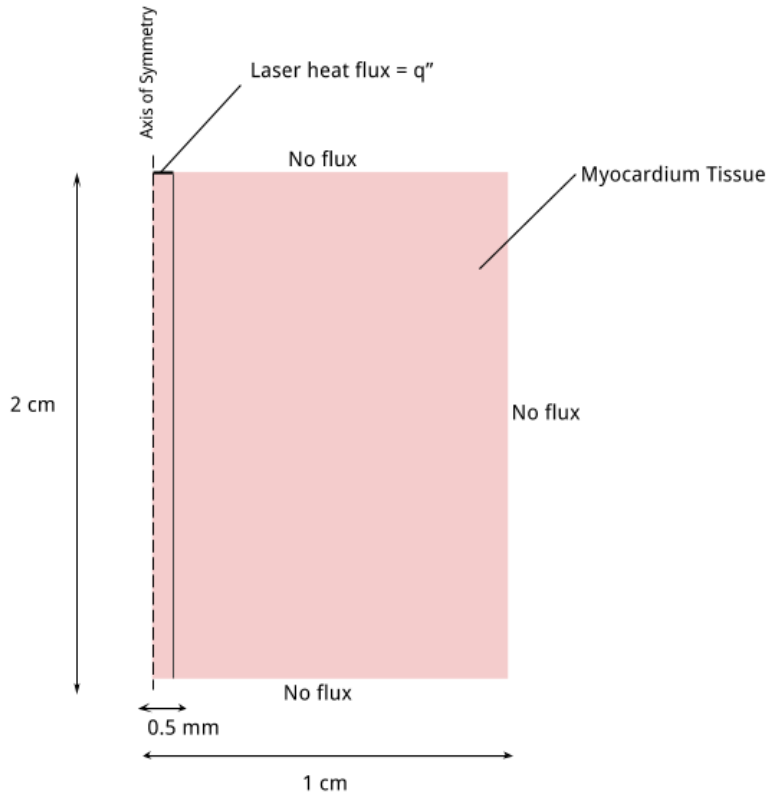

Figure 2: Schematic of laser heating process which will be implemented in COMSOL using a 2-D axisymmetric model. Routinely in TMLR, 1 mm diameter [9] channels are created by the laser. Note the no flux boundaries all around the domain with the exception of the top of the channel where the laser is initially applied with a constant flux.

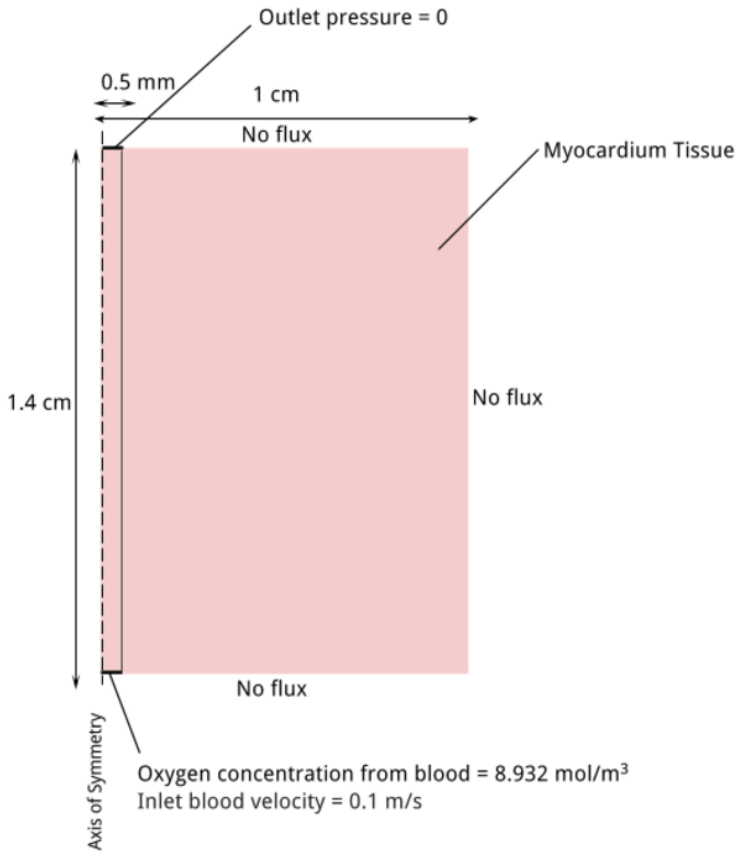

Figure 3: Schematic of oxygenated blood in the channel to illustrate mass flux of oxygen from the blood into the tissue. Take note of the no flux boundary conditions all around the domain except where the channel begins and ends. At the bottom where the tissue comes into contact with the left ventricle, there is a constant concentration boundary condition with inward blood flow. At the top of the channel where the opens up has a no pressure boundary condition to allow unconstrained blood flow.

3.3 Governing Equations

For laser heat diffusion model, we used the heat transfer governing equation in cylindrical coordinates (Equation 1) [10]. We excluded convection and heat generation from our equation since these terms are insignificant compared to the heat coming from the laser power.

$$\rho C_p \frac{\partial T}{\partial t} = k \left[\frac{1}{r} \frac{\partial T}{\partial r} (r \frac{\partial T}{\partial r}) + \frac{\partial^2 T}{\partial z^2} \right] \tag{1}$$

In this equation, ρ , C_p, and k are density, specific heat, and thermal conductivity of the tissue, respectively.

For the mass transfer part of the model, we used the mass transfer governing equation (Equation 2) again in cylindrical coordinates since it can be computed as a 2-D axisymmetric model. We excluded the reaction term, assuming negligible oxygen consumption in the tissue. The blood flow exists only for the channel domain, and thus the equation for the channel domain is

$$\frac{\partial c}{\partial t} + u\frac{\partial c}{\partial z} = D_{O_2,Tissue}\left[(\frac{\partial^2 c}{\partial z^2}) + \frac{1}{r}\frac{\partial c}{\partial r}(r\frac{\partial c}{\partial r})\right] \tag{2}$$

where u is the blood flow velocity and $D_{O_2,Tissue}$ is the diffusivity of oxygen in the myocardium tissue. The tissue domain of the mass transfer model does not have the convective mass transfer term since this domain only relies on the conductive mass transfer for the diffusion of oxygen. The equation for the mass transfer of the oxygen in the tissue domain is

$$\frac{\partial c}{\partial t} = D_{O_2,Tissue}\left[(\frac{\partial^2 c}{\partial z^2}) + \frac{1}{r}\frac{\partial c}{\partial r}(r\frac{\partial c}{\partial r})\right] \tag{3}$$

To model the transient fluid flow effect of the blood flowing in the channel, we have additionally included Navier-Stokes equation (Equation 4) and continuity equation (Equation 5) and coupled it to the mass transfer equation.

$$\rho(u\nabla u) = -\nabla P + \mu\nabla^2 u \tag{4}$$

$$\rho\nabla u = 0 \tag{5}$$

In the fluid flow equations, ρ is the density of the blood, u is the blood inflowing velocity, P is the pressure, and μ is the dynamic viscosity of the blood.

Using these governing equations, the heat and mass transfer of the laser ablation and tissue oxygenation were accurately modeled.

3.4 Boundary Conditions

The boundary conditions for the laser heating model were based on the following assumptions:

1. The right and bottom boundaries have a heat flux of 0 W/m^2, assuming that these surfaces are far away from the heating area (semi-infinite).
2. The top boundary (minus the laser flux boundary) has 0 heat flux.
3. The boundary where the laser heating occurs has a constant heat flux (q") equal to the laser power divided by the laser's cross-sectional area. The laser will ablate the tissue once the tissue reaches the vaporization temperature of 100°C and will create a channel in the negative y-direction as it destroys layers of tissue.
4. Additionally, an ablative heat flux was applied on the same boundary where we applied the laser heat flux (Equation 6). This condition was used to model the removal of the tissue once it reached its vaporization temperature [11].

$$q_a = h_a(T_a - T) \tag{6}$$

Hence, q_a is the heat flux due to tissue ablation; h_a is the heat transfer coefficient as a function of temperature; and T_a is the ablation temperature of 100°C. The heat transfer coefficient for tissue temperatures below vaporization temperature is 0 and is a linear function for tissue temperatures above T_a. This was implemented in COMSOL using a "ramp" function that satisfies the conditions previously stated.

The slope of this function was set to be high so that the temperature of the tissue does not exceed the ablation temperature, enforcing any tissue reaching temperature above 100°C to be removed [11]. Furthermore, this boundary moves in the z-direction at a velocity defined by:

$$v = \frac{q_a}{\rho L} \tag{7}$$

where ρ is the tissue density, L is the latent heat of vaporization, and q_a is the heat flux due to ablation. We assume that the tissue is mostly composed of water, and thus we used the latent heat value for water.

The boundary conditions for the mass transfer model were based on these assumptions:

1. There is no mass flux on the right, bottom, and top sides of the schematic due to a semi-infinite geometry assumption.

$$- D_{O_2,Tissue} \frac{\partial T}{\partial x}\bigg|_{x=0mm} = 0 \frac{W}{m^2} \tag{8}$$

2. There is no flux at the axis due to the symmetry and inability of oxygen to flow past the center.
3. There is a constant oxygen concentration at the inlet of the channel.
4. There is an "open boundary" condition at the outlet of the channel to capture the oxygen concentration in the blood as it blood leaves the channel.

Finally, the boundary conditions for the fluid flow module in the channel were as follows:

1. The inlet velocity of the blood flowing in the channel is fully developed with a parabolic velocity profile and average velocity of 10 cm/s.
2. There is no slip on the channel walls.
3. Outlet pressure of the channel is 0 to allow the blood to flow freely.

3.5 Initial Conditions

- For laser heating:
  Initial temperature everywhere in the heart tissue and blood vessel was 37˚C, the average human body temperature [6].
- For mass transfer:
  Initial oxygen concentration in the tissue was the lethal oxygen concentration c_L whose value is shown in Appendix A.

3.6 Parameters

The parameters inputted for the tissue and blood vessels can be found in Appendix A. The properties of the laser are shown in Table 1.

Table 1: Properties of Laser [12]

Wavelength [μm]	Energy level [$J/pulse$]	Pulse Duration [ms]
10.6	15 to 20	25 to 40

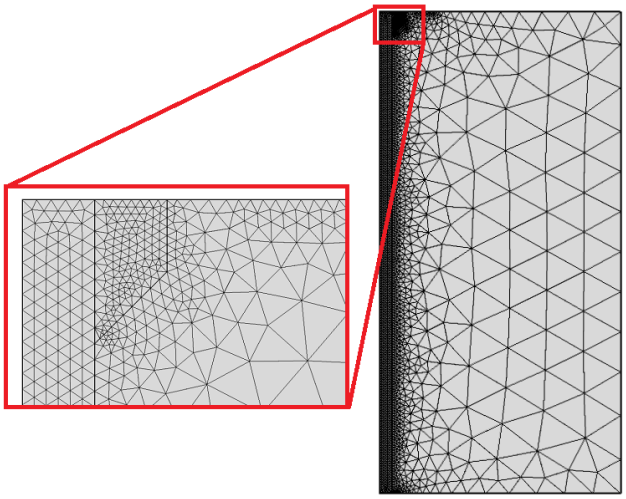

Figure 4: The mesh used for the laser ablation model. The left-most boundary is the axis of symmetry. The interface between the laser pathway and the untouched myocardial tissue had a finer distribution of the mesh since the temperature gradient was largest in the area. This mesh used 4502 elements total. The zoomed in area shows the mesh around the pentagon which was used for average temperature measurements over the area.

4 Results

Upon the specification of the model requirements, the model itself had to be built. During this process, the optimization of the mesh and parameter inputs was required for the removal of discretization errors. Once the model implementation was discretized, the solution optimization could be performed to find the best combination of laser radius and laser power for the least tissue damage and maximum oxygen delivery to the hypoxic tissue.

4.1 Mesh

The development of a reasonable mesh was a crucial step in the model development process. The use of a coarse mesh lacking in a sufficient number of elements is reason for the model to result in a discretization error. Mesh distribution was varied by location such that areas with high concentration gradients had a finer mesh to allow for more frequent computation to insure the heat transfer model was accurate. Figure 4 displays the mesh used in the 2D axisymmetric model for heat transfer in COMSOL. This mesh used a total of 4502 triangular elements, which was determined based on the mesh convergence data.

Implementation of the laser path guide was necessary for the proper ablation of the tissue. Using the deformed geometry module in COMSOL, the area outside of the predetermined

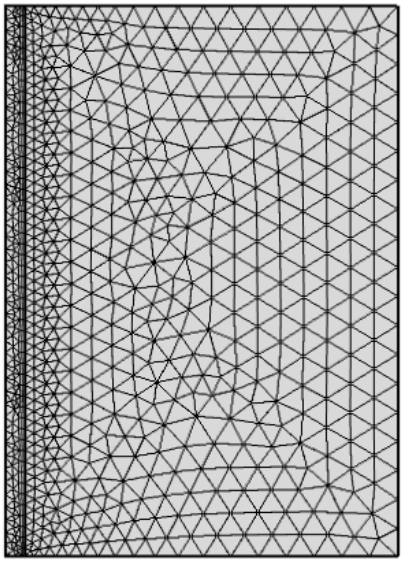

Figure 5: The mesh used for the oxygen transfer model. The left-most boundary is the axis of symmetry. The interface between the channel and the myocardial tissue had a finer distribution of the mesh since the temperature gradient was largest in the area. This mesh used 1627 elements total.

path was assigned a fixed, unmovable mesh. Ablation in this outer area was accounted for later in the objective function in Equation 9. The sides of the channel were only allowed to deform in the z direction, thus ignoring any radial deformation. The tissue inside of the pathway was allowed to deform freely, enabling accurate modeling of the ablation front. Finally, the bottom face of the channel was fixed, while the top face was assigned a "Normal Mesh Velocity," using (Equation 7). The preset path thus allowed for the ablation of the desired channel and did not hinder heat transfer beyond the boundary of the pathway and was therefore deemed appropriate.

The mesh for the mass transfer was developed similarly to the heat transfer mesh in that it required a finer mesh in the channel portion due to the greater oxygen concentration gradient. Figure 5 is an image of the final mesh chosen for the mass transfer. Fluid flow was implemented in the channel portion of the mesh.

4.1.1 Heat Transfer Mesh Convergence

The monitored parameter for the mesh convergence of our model was an average temperature over the pentagonal area near the surface of the tissue shown in Figure 6. The basis on which the area was chosen was that the area had to be close to the top of the tissue where the laser initially begins ablation since that is where the greatest temperature gradient exists, making this an area of interest for monitoring temperature changes depending on parameter variation. Taking this condition into account, the chosen area was a pentagon right outside the channel and slightly below the top of the tissue as shown in Figure 6. The outermost line lies at $r = 0.001m$ with a length of 0.0005 m and the line in contact with the channel border begins at the top of the tissues and has a length of 0.001 m. A pentagon was the geometry of choice due to the radial heat transfer that occurred at the beginning of the process due to the initial contact of the laser with the tissue at the top

of the domain, and the decreasing temperature profile as distance from the top increases.

The temperature profile of the average over this area was taken for multiple meshes for the mesh convergence analysis as shown in Figure 7. Five meshes with increasing element count yielded a convergence to a solution. The results suggested that it was not necessary to compute any further refined meshes. Looking at the resulting graphs, lower quality meshes result in unphysical variations in the solutions, while the higher qualities yield a smooth curve, as expected. With an increase of 900 elements from the 4502 element mesh to the 5473 element mesh, solutions are almost identical, suggesting convergence of the meshes. Thus, the discretization errors will mostly be able to be avoided using the 4502 element mesh in order to minimize data usage and computation time since the 5473 element mesh computation takes an hour longer to compute a comparable solution.

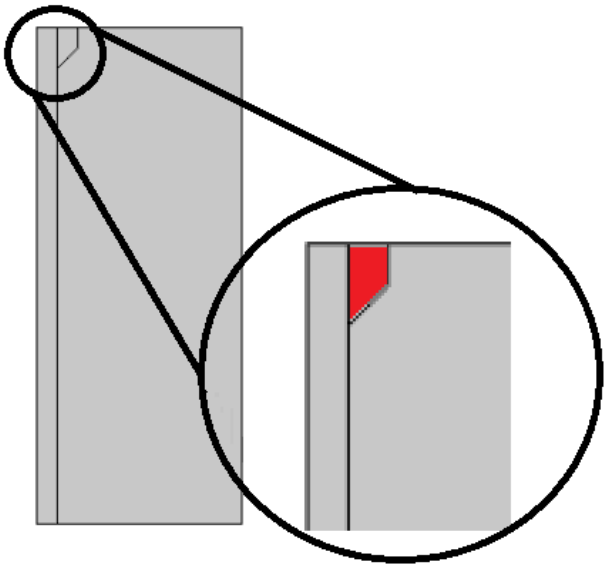

Figure 6: Polygonal average temperature calculation area. The figure shows the domain alongside an enlarged image of the portion of the tissue where the average surface temperature was taken for the sensitivity analysis. The shaded polygonal red region is the area of interest.

The resulting heat transfer 3D temperature plot using the chosen mesh is shown in Figure 8. This zoomed in image shows the only part of the domain where the temperature spike occurred beyond the radius of the specified channel.

4.1.2 Mass Transfer Mesh Convergence

The mesh convergence for the 2-D axisymmetric oxygen mass transfer portion of the project resulted in apparent convergence of all meshes tested. The mesh convergence was a result of a cut point temperature plot at $r = 0.0005m$ and $z = 0.01m$ in the 2-D model. This is the point at the middle of the tissue at the interface where the channel and tissue meet. As seen in Figure 9, the similarity in results regardless of the mesh size is most likely due to the simplicity of this model. Based on these results, the decision to move forward using the mesh with the lowest number of elements within the convergence regime was made in order to minimize computation while obtaining an accurate result.

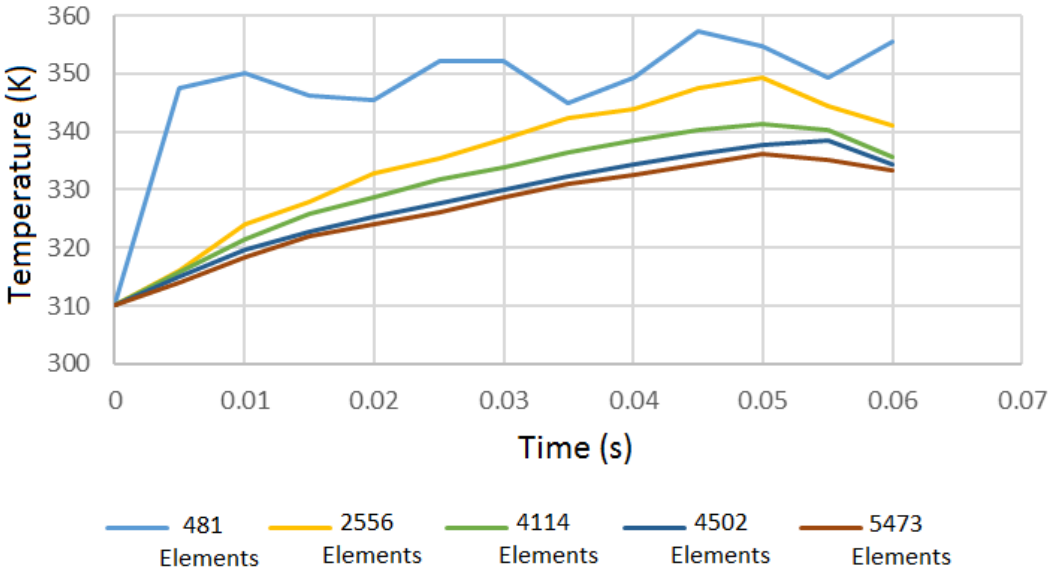

Figure 7: Heat transfer mesh convergence. As the number of elements in the mesh increases, the temperature profile for the average temperature taken over the pentagonal area converges.

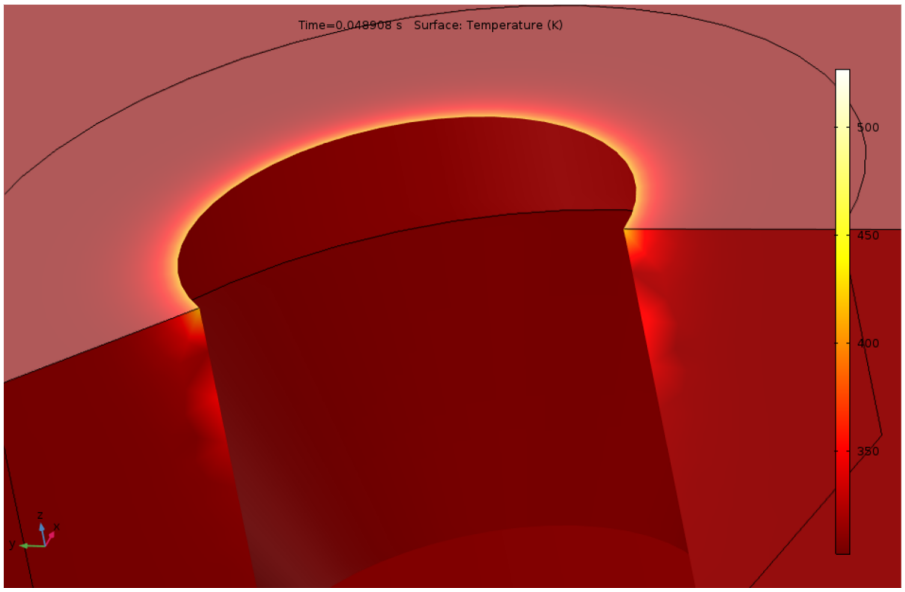

Figure 8: Zoomed image of the solution. After discretization of the mesh, this 3D temperature plot resulted. This plot is zoomed into the area where the laser initially came into contact with the tissue, at the top of the domain. This was the only area where the heat transfer was visible since the rest of the domain was ablated as soon as it was heated.

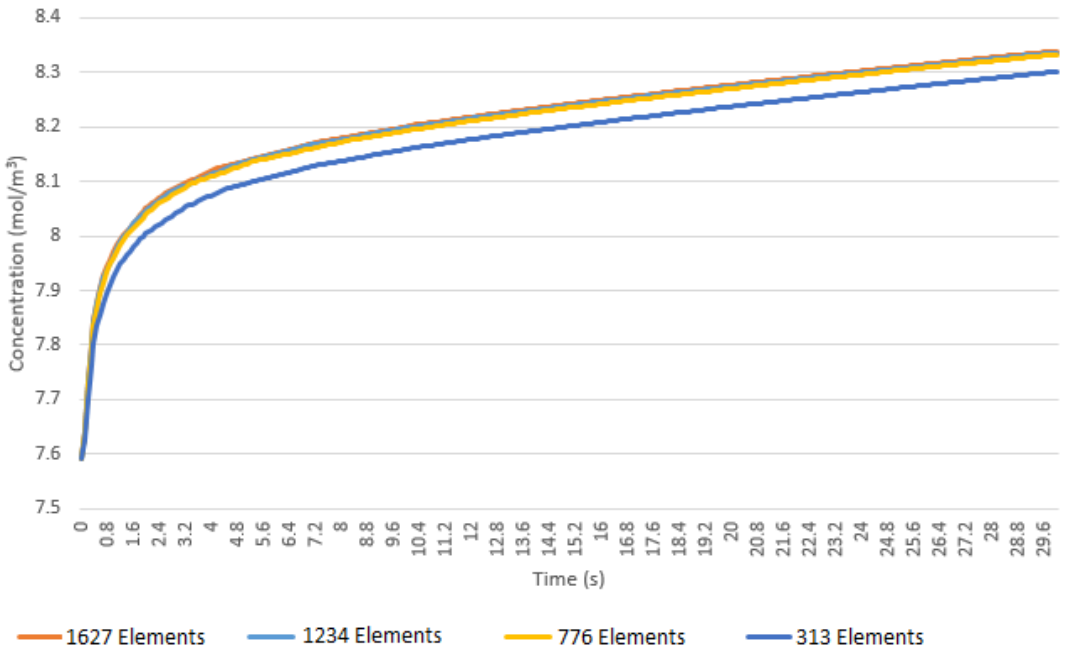

Figure 9: Mass transfer mesh convergence. The meshes for the oxygen mass transfer through the new blood vessel converge when the mesh has above 776 elements. The convergence plot was taken as a result of a cut-point concentration over time in the 2-D axisymmetric model. The cut point was taken at r = 0.0005m and z = 0.01m.

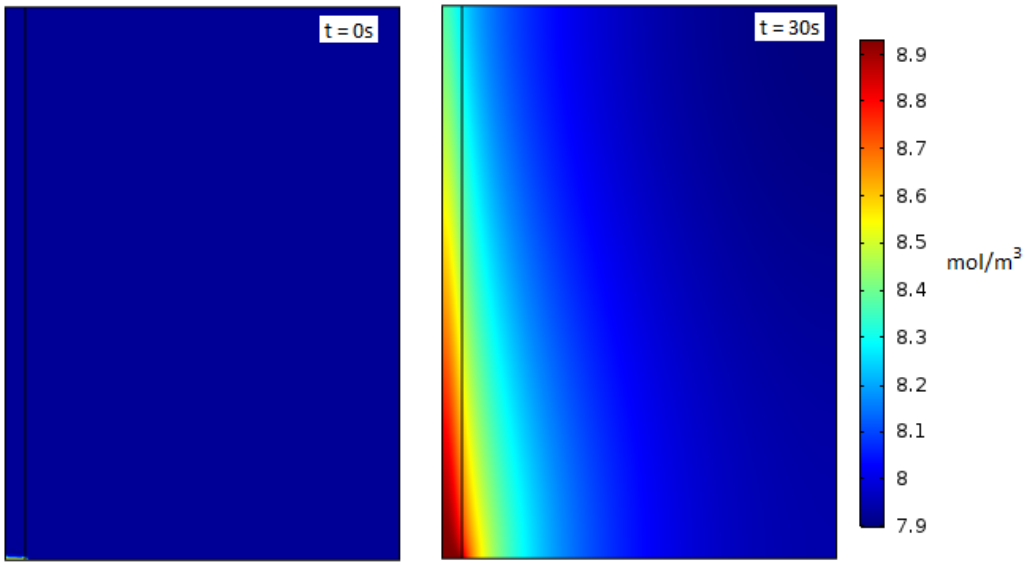

Figure 10: The 2-D axisymmetric mass transfer surface plots at time 0s and 30s after discretization of mesh. The oxygen transfer with fluid flow greatly increases the oxygenation of the tissue within a span of 30 seconds.

After discretization of the mesh for the mass transfer model, the surface plots of the mass transfer were obtained as shown in Figure 10. The oxygen concentration increases from 7.593 $\frac{mol}{m^3}$ over the whole domain to an average concentration of 8.355 $\frac{mol}{m^3}$.

4.2 Sensitivity Analysis

Computational models must be able to compute realistic and accurate solutions regardless of variability in the parameter inputs. Sensitivity analyses were conducted to determine the percent change impact that percent change variability in each input parameter has on each of the heat transfer and mass transfer models. Four variables were manipulated in the heat transfer model while two variables were manipulated in the mass transfer model.

4.2.1 Heat Transfer Sensitivity Analysis

For the sensitivity analyses of the heat transfer model, twenty percent changes in thermal conductivity, density, and specific heat of the tissue and the flux of the laser were applied. The effect of these changes were then monitored by evaluating the percent change in average temperature in our critical area located near the top of the tissue, with a spot size radius of $r = 0.0005m$.

Altering the thermal conductivity affects the temperature of the tissue because it is directly related to conduction in the heat transfer governing equation. However, as seen in Figure 11, thermal conductivity has essentially no effect on the average temperature in that region. This can be attributed to the fact that conduction has little time to occur due to the very short time of the procedure and the speed at which the heat boundary is moving downwards.

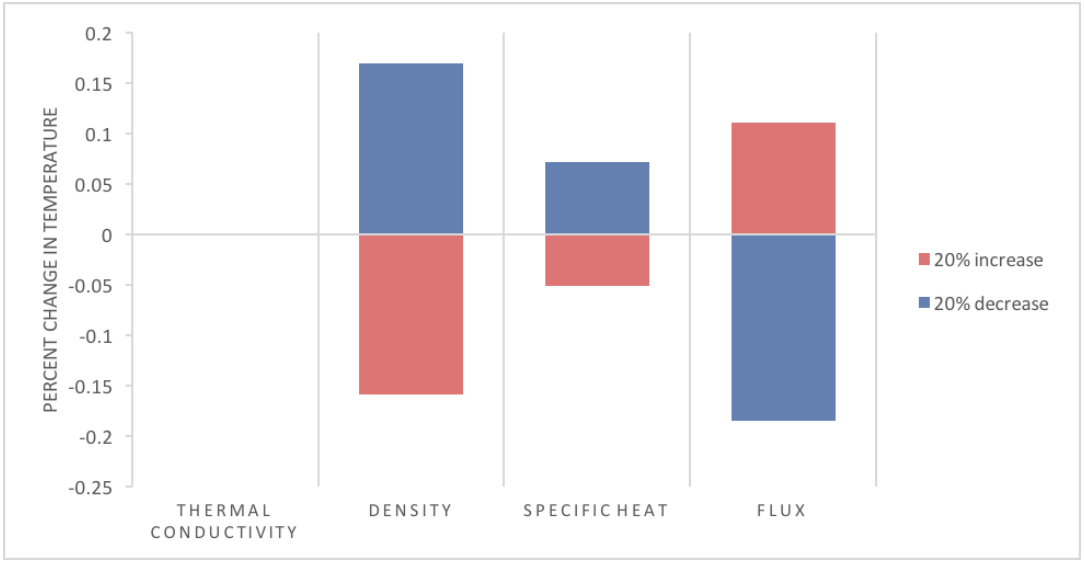

Figure 11: The plot above shows the relative changes in average temperature over our critical region after increasing and decreasing the parameters shown by twenty percent from the default. All the parameters above have little effect on the average temperature in that region, with a maximum of around 0.2 percent change in the average temperature.

Heat capacity is directly correlated to how much energy is required for the tissue to change temperatures. Thus, changing the heat capacity was hypothesized to have an effect on the temperature of the point. This is observed in Figure 11, but to little extent, resulting in at most 0.1 percent change of average temperature. Again, due to the low total procedure time, we understood that heat capacity's effect on temperature would consequentially be minimal.

Density of the tissue is an intrinsic property of the tissue that affects the temperature of the ablation. Physically speaking, the density of the material being ablated affects the velocity of ablation due to the greater amount of material that the laser heat must vaporize before moving forward. Therefore it is logical that a twenty percent increase in density would decrease temperature in our region of interest, as seen in the figure.

Finally, we observed changes in the average temperature over the specified area as we changed the value of the heat flux. As seen in Figure 11, an increase in flux induced a small change in average temperature. As mentioned before, since conduction is playing a small role, the increase in temperature would most likely be larger if our critical region was defined smaller. This effect of flux on temperature was revisited thoroughly in our optimization of the model.

Overall, the relative changes in these four parameters offered some credit to their significance, but more importantly their small percentage influence on average temperature in the region of interest showed the minimal role conduction plays in TMLR.

4.2.2 Mass Transfer Sensitivity Analysis

The concentrations for the sensitivity analyses were taken at the cut point $r = 0.005m$ and $z = 0.001m$, at the last time point, $t = 30seconds$.

Diffusion coefficient of oxygen through the tissue had a direct effect on mass transfer. The diffusion coefficient is a parameter that describes the ability of one species to pass through another medium by diffusion. Thus, a higher diffusion coefficient indicates that the species is able to diffuse through a specific material faster than a species with a lower value of diffusivity. This hypothesis was supported by the results of the sensitivity analysis shown in Figure 12, which showed that a twenty percent increase in diffusion coefficient led to a 0.5 percent increase in average concentration.

Variation in the blood flow velocity through the channel affected the concentration gradient because the flow of blood is what causes the replacement of oxygen particles in the channel, allowing for more oxygen to be provided to the tissue. Thus, a higher velocity is naturally able to deliver the oxygen that diffuses through the tissue faster. This idea was supported by the sensitivity analysis shown in Figure 12.

Overall, the mass transfer sensitivity analysis showed that neither of the parameters provided were sensitive to changes. This indicated that the model is feasible for almost any value of these parameters without drastically affecting the solution.

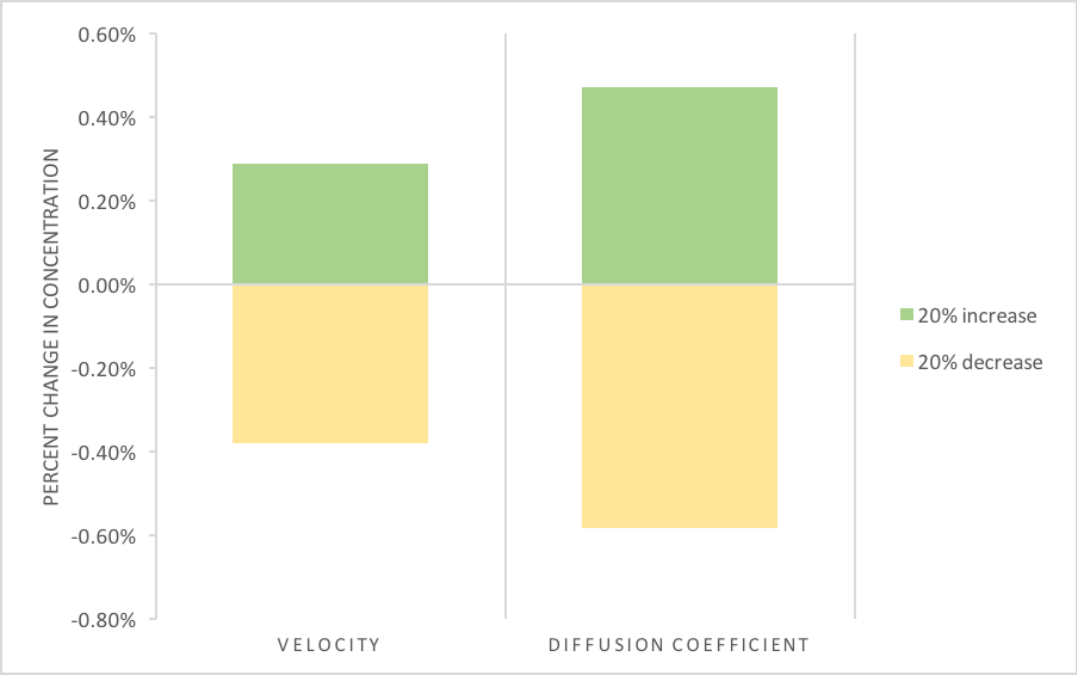

Figure 12: The plot above shows the relative changes in oxygen diffusion after increasing and decreasing the blood flow velocities and oxygen diffusivity of the tissue by twenty percent each.

4.3 Solution Optimization

Our optimization involved the monitoring of the tissue within a set radius around the cylindrical volume of the laser probe to see that the volume of damaged tissue outside the desired ablation volume is minimized while maximizing oxygenation. The flux can be calculated by dividing the laser power by the cross sectional area of the laser-front [12]. Tissue damage was defined to occur when the tissue reached a temperature of 60°C [13]. An objective function was implemented to determine the most optimal combination of laser power and laser radius. Thus, the goal of the objective function (J) was to minimize the value.

$$J = \sum_{i=1}^{n} \begin{Bmatrix} 50 & T \geq 373K \\ 30 & 373K > T \geq 333K \\ 0 & 333K > T \end{Bmatrix} \times \left(1 + \frac{C_{min} - C}{C_{min}}\right) \tag{9}$$

Here, C_{min} is the minimum viable oxygen concentration indicated in Appendix A and C is the average oxygen concentration over the whole domain after 30 seconds.

After applying this optimization function to the solution and applying a parametric sweep for different laser radii and laser powers, we obtained the graph shown in Figure 13. Since the goal of the objective function was to minimize the J value, the most optimal condition is represented by the lowest value on the graph. The optimal radius corresponded to $r = 0.55mm$. Within this radius, the optimal applied power was any power between 538 W and 600 W since the objective function value was unaffected between those power values.

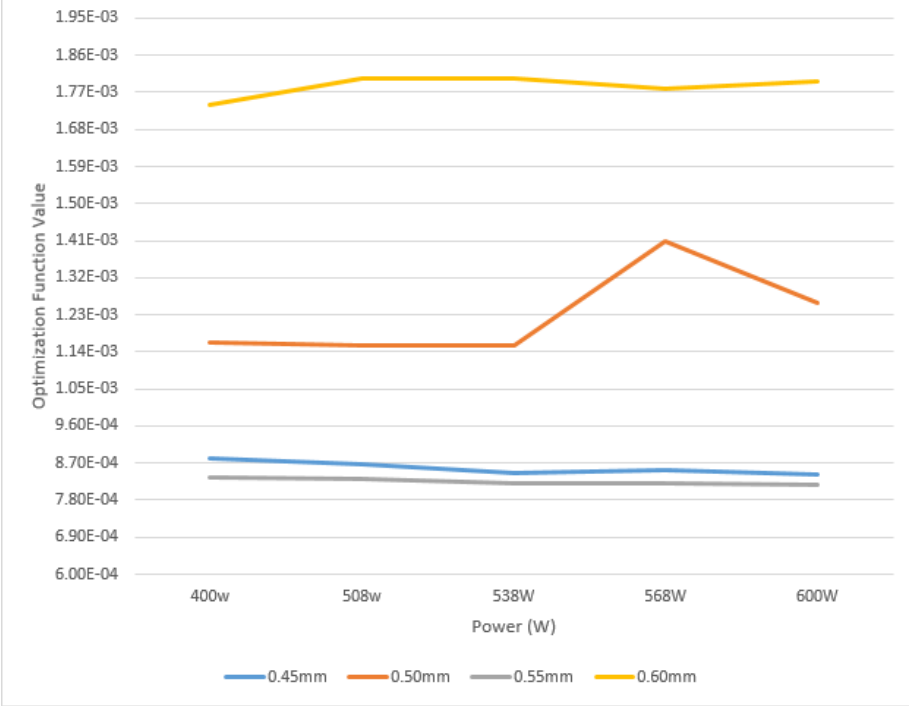

Figure 13: The plot shows the solution optimization using the objective function defined in Equation 9. Each line represents a different laser radius while the x-axis varies the laser power applied to the tissue. The optimal radius and power combination appears to be a radius of $r = 0.55mm$ *and any power between* $538W$ *and* $600W$

5 Discussion

The solution obtained upon performing the mesh convergence, sensitivity analysis, and solution optimization cannot easily be accepted. It must undergo data validation as a final step of verifying the solution.

5.1 Data Validation

To validate our heat transfer model, we compared the ablation time (the time it takes to make one channel through the myocardium wall thickness) of our model to the laser pulse time in literature. In the real-life procedure, a single laser pulse is used with the CO_2 laser, and each pulse duration ranges from 25 to 40 ms to make the channel [14]. The ablation time from our heat transfer model was 55.9 ms as seen in Figure 14. Although our model's procedure time was outside of the literature time range, the ablation time still seemed reasonable and was in the same magnitude as the literature time. Thus, we concluded that the model ablation time was close to the literature value and that our heat transfer model was validated. Qualitatively, the solution appeared to be accurate in that the top surface where the laser flux was applied had the highest temperatures while the surrounding tissue remained at the initial body temperature. Since the laser moves very quickly due to the high laser heat flux, the procedure can be completed very rapidly. This speed diminishes the effects of heat conduction. The same phenomena was observed in our model, in which the area around the channel was still at body temperature because of minimal heat conduction.

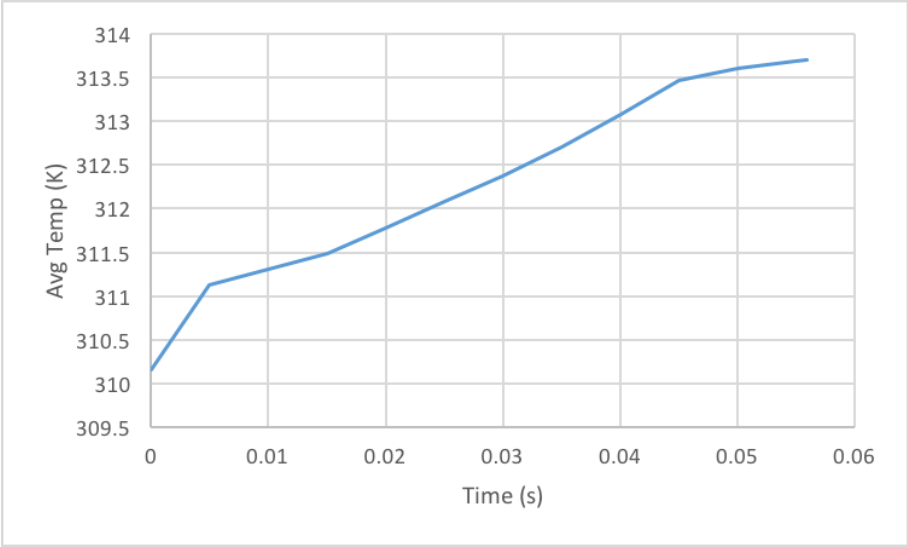

Figure 14: This plot shows the average temperature in the defined region vs time for applied power of 538 W and a laser radius of 0.5 mm. The line stops at a time of 0.0559s, showing that our ablation time was 55.9 ms.

Validation for our mass transfer model was more challenging, as most literatures measured physical improvements in patients to determine the efficacy of TMLR. One study, however, measured the intramyocardial partial pressure of oxygen ($p_{ti}O_2$) at different time intervals of several patients who had undergone the TMLR procedure [15]. After 1 hour, the average $p_{ti}O_2$ of the patients reached 17.8 mmHg from the baseline (pre-operative) level of 12.3 mmHg, displaying a significant increase in oxygen level in the short amount of time [15]. To connect $p_{ti}O_2$ measurements with our model, we looked at another literature that focused on relating arterial partial pressure of oxygen to the myocardial partial pressure of oxygen of dogs [16]. In this article, the average myocardial pO_2 of dogs with the "healthy" and "viable" arterial pO_2 were 19.3 mmHg and 18.9 mmHg, respectively. These values are similar to the 17.8 mmHg $p_{ti}O_2$ mentioned in the previous paper, indicating that the average patient who had undergone the TMLR procedure had reached the viable oxygen level in the heart in the short term. Likewise, our mass transfer model demonstrated that most of the cardiac tissue reached the viable oxygen concentration or beyond after 30 seconds the channel has been created. Since no literature would look at a patient's oxygen level 30 seconds after the surgery, and 1 hour post operation data was the best we could find, we made a general conclusion that our model is valid for demonstrating the short-term efficacy of TMLR.

6 Conclusion

The resulting oxygenation of the initially hypoxic myocardium (7.593 $\frac{mol}{m^3}$) achieved an an oxygen concentration of 8.355 $\frac{mol}{m^3}$ in a short time span of 30 seconds. This oxygen concentration was above the minimum viable oxygen concentration of 8.039 $\frac{mol}{m^3}$ meaning that this volume of the patient's heart tissue returned to a relatively stable state within 30 seconds. Though the short-term oxygenation process does not allow the tissue to reach the normal oxygen concentration of 8.932 $\frac{mol}{m^3}$, the patient only requires the minimum

viable concentration for the time being in order to maintain viable oxygen concentration until angiogenesis allows for continuous, long-term oxygenation of the tissue.

6.1 Design Recommendations

According to the optimization function, the optimal combination of power and channel radius is between 538 W and 600 W and 0.55 mm, respectively. Operating at this power and radius yielded an ablation pulse time of 55.9 ms.This optimization allowed for minimized healthy tissue damage while maximizing the subsequent oxygen flow that occurs through the ablated channel. Though any laser power between the indicated values are sufficient for the procedure, it is recommended to use a laser power as close to 538 W as possible in order to minimize the risk of overheating and reduce economic constraints such as operational and energy costs. The resulting oxygenation of the initially hypoxic myocardium (7.593 $\frac{mol}{m^3}$) achieved an an oxygen concentration of 8.355 $\frac{mol}{m^3}$ in a short time span of 30 seconds. Abiding by these CO_2 laser design recommendations should yield a TMLR procedure with minimized tissue damage and maximized tissue oxygenation.

7 Appendix A: Input Parameters

Properties of the myocardial tissue, blood and blood vessel and properties relevant to each material are listed in the table below.

Table 2: Properties of Biological Materials

Tissue	Parameter [symbol]	Value [Unit]	Reference
Myocardium	Thermal Conductivity [k]	0.493 [$\frac{W}{mK}$]	[13]
	Thermal Diffusivity [α]	1.474E-7 [$\frac{m^2}{s}$]	[16]
	Diffusivity of Oxygen [$D_{O_2,Tissue}$]	2.4E-6 [$\frac{m^2}{s}$]	[18]
Blood Vessel	Thermal Conductivity [k_v]	0.5 [$\frac{W}{mK}$]	[19]
	Specific Heat [C_p]	3900 [$\frac{J}{kgK}$]	[19]
	Density [ρ]	1060 [$\frac{kg}{m^3}$]	[19]
Blood	Thermal Conductivity [k_B]	0.492 [$\frac{W}{mK}$]	[20]
	Specific Heat [C_p]	3900 [$\frac{J}{kgK}$]	[19]
	Density [ρ]	1060 [$\frac{kg}{m^3}$]	[19]
	Flow Velocity [v]	0.1 [$\frac{m}{s}$]	[21]
	Normal Oxygen Concentration [c_n]	8.932 [$\frac{mol}{m^3}$]	[22]
	Minimum Viable Oxygen Concentration [c_m]	8.039 [$\frac{mol}{m^3}$]	[22]
	Lethal Oxygen Concentration [c_L]	7.593 [$\frac{mol}{m^3}$]	[23]
	Oxygen Flux [Φ]	18.955 [$\frac{mol}{m^2 s}$]	[24]

8 Appendix B: Computational Methods

Version 5.2a of COMSOL Multiphysics was used to develop the model. This appendix details the computational input methods used for the models.

```
Stop condition fulfilled at t = 0.048926 (Stop expression 1).
Time-Dependent Solver 1 in Study 1/Solution 1 (sol1): Solution time: 990 s (16 minutes, 30 seconds)
                                                      Physical memory: 1.37 GB
                                                      Virtual memory: 1.47 GB
```

Figure 15: Screenshot of the run log for the heat transfer model. The optimized heat transfer model took 16 minutes and 30 seconds to compute and used 1.47 GB of memory.

```
Time-Dependent Solver 1 in Study 1/Solution 1 (sol1): Solution time: 4 s
                                                      Physical memory: 1.14 GB
                                                      Virtual memory: 1.27 GB
```

Figure 16: Screenshot of the run log for the mass transfer model. The optimized mass transfer model took 4 seconds to compute and used 1.27 GB of memory.

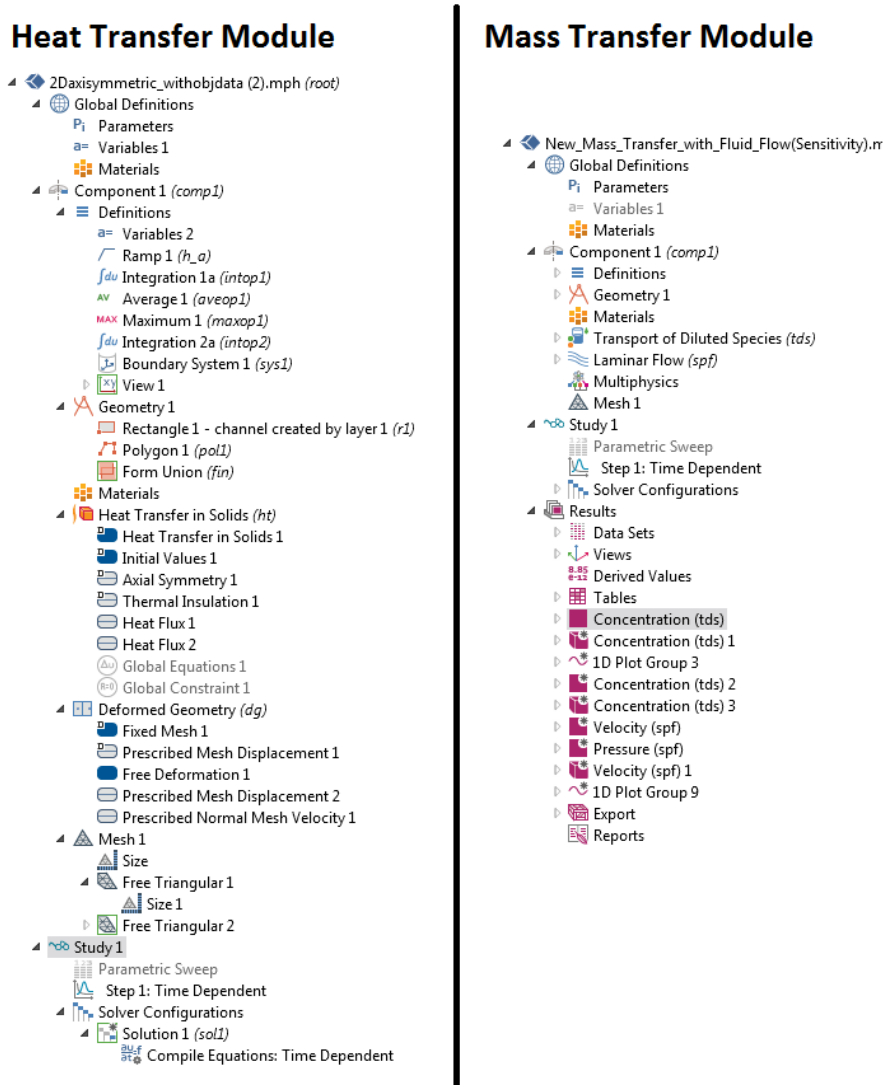

Figure 17: Screenshot of the heat transfer and mass transfer model builder bars. On top of the regular modules, the heat transfer model used the deformed geometry module and a stop condition. A closer view of the deformed geometry and stop condition implementations can be seen in Figures 18 and 19. The mass transfer model did not use any significantly different modules.

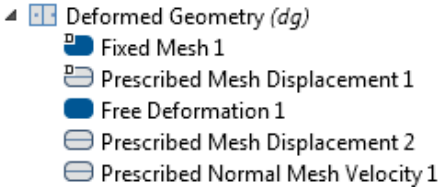

Figure 18: Zoomed in view of the deformed geometry model builder tab. The deformed geometry module was a challenge due to the massive amount of deformation our model had to accommodate.

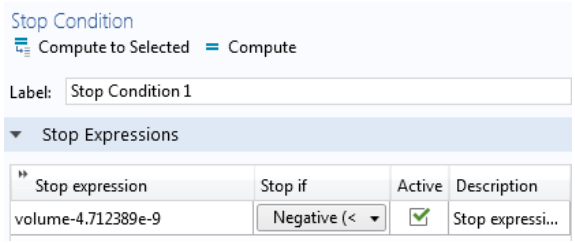

Figure 19: Screenshot of the stop condition implementation for the heat transfer model. This stop condition was used to stop the laser ablation process once the laser reached the end of the tissue.

References

1. M. Mirhoseini and M. M. Cayton, "Revascularization of the heart by laser," *Microsurgery*, vol. 2, no. 4, pp. 253-260, 1981.
2. University of Michigan School of Medicine. (December, 2015), "Bypass Grafting," [Online]. Available: http://surgery.med.umich.edu/vascular/patient/ treatments/ bypass.shtml, Mar. 2, 2017.
3. J. Iwanski et. al., "Remodeling an infarcted heart: novel hybrid treatment with transmyocardial revascularization and stem cell therapy". *SpringerPlus*, vol. 5, no. 1, pp. 738, 2016. DOI: 10.1186/s40064-016-2355-6.
4. O. Soran, "Alternative therapy for medically refractory angina: enhanced external counterpulsation and transmyocardial laser revascularization," *Cardiology Clinics*, vol. 32, no. 3, pp. 429-438, 2014.
5. L. Han, S. Guo, and W. Xu, "Design of clinical intelligent percutaneous myocardial laser revascularization operating platform software," MATEC Web of Conferences vol. 40, Jan. 2016.
6. N.B. Schiller, et. al.,(1989). "Recommendations for quantitation of the left ventricle by two-dimensional echocardiography," *Journal of the American Society of Echocardiography*, vol. 2, no. 5, pp. 358-367, 1989.
7. R.B. Devereux, "Echocardiographic assessment of left ventricular hypertrophy: comparison to necropsy findings," *The American Journal of Cardiology*, vol. 57, no. 6, pp. 450-458, 1986.
8. Icahn School of Medicine at Mount Sinai, (2017). "Transmyocardial Laser Revascularization," [Online]. Available: https://www.wehealny.org/services/ bi-cardiacsurgery/ revascularization.html, Apr. 03, 2017.
9. K.A. Horvath, "Transmyocardial laser revascularization," *Journal of Cardiac Surgery*, vol. 23, no. 3, pp. 266-276, 2008.
10. A.K. Datta, "Biological and bioenvironmental heat and mass transfer," CRC Press, 2002.
11. COMSOL Blog, (2016). "Modeling Thermal Ablation for Material Removal," [Online]. Available: https://www.comsol.com/blogs/modeling-thermal-ablation-for-material-removal/, Apr. 23, 2017.

12. Synrad "10.2 Micrometer Series Laser," [Online]. Available: http://www. synrad. com/10-2Series/index.html, Mar. 03, 2017.

13. C. Rossmann, and D. Haemmerich, "Review of temperature dependence of thermal properties, dielectric properties, and perfusion of biological tissues at hyperthermic and ablation temperatures," *Critical Reviews in Biomedical Engineering*, vol. 42, no. 6, 2004.

14. B. A. Kindzelski, Y. Zhou, and K. A. Horvath, "Transmyocardial revascularization devices: technology update," *Medical devices* (Auckland, NZ), 8, 11, 2015.

15. M. Misfeld, J. U. Rhau, H. H. Sievers, and E. G. Kraatz, "Intramyocardial partial oxygen pressure in patients undergoing transmyocardial laser revascularization and bypass surgery," Scandinavian Cardiovascular Journal, vol. 37, no. 5, pp. 270–274, Sep. 2003.

16. B. Losse, S. Schuchhardt, and N. Niederle, "The oxygen pressure histogram in the left ventricular myocardium of the dog," Pflugers Archiv European Journal of Physiology, vol. 356, no. 2, pp. 121–132, 1975.

17. J. D. B. MacDougall, and M. McCabe, "Diffusion coefficient of oxygen through tissues," *Nature*, vol. 215, no. 5106, pp. 1173-1174, 1967.

18. Q. Fang, et. al., "Oxygen advection and diffusion in a three-dimensional vascular anatomical network," *Optics Express*, vol. 16, no. 22, pp. 17530-17541, 2008.

19. E. Majchrzak and D. Tarasek, "Numerical modeling of heat transfer in a single blood vessel and surrounding biological tissue", *Scientific Research of the Institute of Mathematics and Computer Science*, vol. 9, no. 2, pp. 145-152, 2010.

20. K.R. Holmes, "Thermal Properties," [Online]. Available: http://users. ece.utexas. edu/ valvano/research/Thermal.pdf Apr. 10, 2017.

21. I.T. Gabe, "Measurement of instantaneous blood flow velocity and pressure in conscious man with a catheter-tip velocity probe," *Circulation*, vol. 40, no. 5, pp. 603-614, 1969.

22. F. J. Giordano, "Oxygen, oxidative stress, hypoxia, and heart failure," *The Journal of Clinical Investigation*, vol. 115, no. 3, pp. 500-508, 2005.

23. M. A. Rodrigues, "Physiological and hypoxic oxygen concentration differentially regulates human c-Kit+ cardiac stem cell proliferation and migration," *American Journal of Physiology-Heart and Circulatory Physiology*, vol. 311, no. 6, pp. H1509-H1519, 2016.

24. University of Texas "Gas Carriage: Oxygen," [Online]. Available: http://www.ld99.com/reference/old/text/2878909-274.html, May 02, 2017.